OPEN ACCESS
IOP Publishing | IMMT
International Journal of Extreme Manufacturing
Int. J. Extrem. Manuf. **2** (2020) 045102 (17pp)
https://doi.org/10.1088/2631-7990/abab4a

Surface defects incorporated diamond machining of silicon

Neha Khatri[1], Borad M Barkachary[2], B Muneeswaran[3], Rajab Al-Sayegh[4], Xichun Luo[5] and Saurav Goel[6,7,8,9]

[1] Optical Devices & System Division, CSIR-CSIO, Sector 30, Chandigarh, 160030, India
[2] Department of Mechanical Engineering, Jorhat Institute of Science & Technology, Jorhat Assam 785010, India
[3] Fenner Conveyor Belting Pvt. Ltd., Dindigul Road Nagri, Madurai, Vadipatti Taluk 625 221, India
[4] College of Engineering, Northern Border University, Arar 91431, Saudi Arabia
[5] Centre for Precision Manufacturing, DMEM, University of Strathclyde, Glasgow G1 1XQ, United Kingdom
[6] School of Engineering, London South Bank University, 103 Borough Road, London SE1 0AA, United Kingdom
[7] EPSRC Centre for Doctoral Training in Ultra-Precision Engineering, University of Cambridge and Cranfield University, Cranfield, United Kingdom
[8] School of Aerospace, Transport and Manufacturing, Cranfield University, Bedfordshire MK43 0AL, United Kingdom
[9] Department of Mechanical Engineering, Shiv Nadar University, Gautam Budh Nagar 201314, India

E-mail: nehakhatri@csio.res.in, borad.barkachary@gmail.com, munees75@gmail.com, rajab.alsayegh@nbu.edu.sa, xichun.luo@strath.ac.uk and goels@lsbu.ac.uk

Received 15 May 2020, revised 9 June 2020
Accepted for publication 31 July 2020
Published 2 September 2020

Abstract

This paper reports the performance enhancement benefits in diamond turning of the silicon wafer by incorporation of the surface defect machining (SDM) method. The hybrid micromachining methods usually require additional hardware to leverage the added advantage of hybrid technologies such as laser heating, cryogenic cooling, electric pulse or ultrasonic elliptical vibration. The SDM method tested in this paper does not require any such additional baggage and is easy to implement in a sequential micro-machining mode. This paper made use of Raman spectroscopy data, average surface roughness data and imaging data of the cutting chips of silicon for drawing a comparison between conventional single-point diamond turning (SPDT) and SDM while incorporating surface defects in the (i) circumferential and (ii) radial directions. Complementary 3D finite element analysis (FEA) was performed to analyse the cutting forces and the evolution of residual stress on the machined wafer. It was found that the surface defects generated in the circumferential direction with an interspacing of 1 mm revealed the lowest average surface roughness (Ra) of 3.2 nm as opposed to 8 nm Ra obtained through conventional SPDT using the same cutting parameters. The observation of the Raman spectroscopy performed on the cutting chips showed remnants of phase transformation during the micromachining process in all cases. FEA was used to extract quantifiable information about the residual stress as well as the sub-surface integrity and it was discovered that the grooves made in the circumferential direction gave the best machining performance.

2631-7990/20/045102+17$33.00

The information being reported here is expected to provide an avalanche of opportunities in the SPDT area for low-cost machining solution for a range of other nominal hard, brittle materials such as SiC, ZnSe and GaAs as well as hard steels.

Supplementary material for this article is available online

Keywords : surface defect machining, silicon, finite element analysis, surface roughness

(Some figures may appear in colour only in the online journal)

1. Introduction

Silicon has been the prime material of modern optics/photonics due to its unique engineering characteristics. The utilisation of silicon is ubiquitous in the field of optoelectronics, MEMS, space and defence industries. The drive for miniaturisation in the production of gadgets making use of silicon is now requiring reduced energy consumption and faster productivity to produce silicon optics. Considerable research work on silicon has been done that has advanced our understanding of this topic since the 1990s. For example, Blackley *et al* [1] gave a fundamental understanding of ductile mode machining of germanium using the single-point diamond turning (SPDT) process.

Shibata *et al* [2] examined the critical influence of the crystallographic orientation on the finished machined surface and concluded that the (111) surface of silicon offers the best machinability. It was proposed that the ductility observed during micromachining of silicon is broadly an outcome of the high-pressure phase transformation (HPPT) [3]. Using Raman spectroscopy, it was demonstrated that the stress state in silicon during cutting causes the diamond cubic (α-silicon) structure to undergo a metastable body centred tetragonal (β-silicon) structural transformation and then depending on the release of strain rate (or cutting speed), the ductile phase back-transforms to the amorphous room temperature phase of silicon. More recently, a direct amorphization without any prior Si-II transition observed from the MD simulation was also proposed to be another ductility mechanism [4]. However, a key problem during SPDT is the in-process degradation and wear of the diamond tool causing worsening of the quality of the machined surface. It is widely known that the wear volume of the diamond tool scales with the cutting distance and that the tool's flank face undergoes relatively more wear than its rake face [5, 6].

In an attempt to improve the machinability of difficult-to-cut, hard and brittle materials like silicon, a range of performance enhancement methods have been proposed and augmented in recent times including the incorporation of laser, cryogenic and electroplasticity concepts [7], all these hybrid and sequential micromachining approaches possess their distinct advantages.

Surface defect machining (SDM) is a recent advancement that was explicitly reported for improving the quality of hard turning during cutting of hard steels of up to 69 HRC [8–10]. Lately, the insights obtained from molecular dynamics simulation study on processing silicon carbide (SiC) hinted at exploiting this route even for the machining of hard, brittle materials [11]. The MD simulation results showed that the surface defects bring a reduction in shear plane angle, shear plane area and side flow with less metallurgical transformations [11]. Hard, brittle materials usually possess low fracture toughness and silicon is by far the most classic example. Built on previous learnings about SDM, this feasibility study was performed to evaluate the quality of machining in SPDT of the silicon wafer. The aim was to quantify the performance improvement in the extent of residual stresses, improved tool life and ultimately to achieve an improved machined surface finish through the SPDT method with the view of eliminating the need for post-machining polishing.

In particular, this paper expands the idea of the SDM method in the SPDT context, which in essence is an expansion of the pulse laser pre-treated machining method [12]. Recently, a smoothed particle hydrodynamics study on SDM on silicon reported reduced cutting pressure [13]. However, experimental evidence is lacking as this is the first paper experimentally demonstrating the surface defect micromachining of silicon.

Another motive behind this work was to select the shape of surface patterns in such a way that the time to produce the surface defects can be reduced and to make it convenient and cost-efficient. It may be recalled from the aforementioned papers that the surface defects can be generated either by conventional mechanical methods or by using a laser. This work produced these defects using the same SPDT machine with the diamond tool itself just prior to machining. Thus, it saved using any additional machine tool or instrumentation. The experimental results thus obtained were complimented by numerical finite element analysis (FEA) to demonstrate the salient aspects concerning the effectiveness of the proposed surface defect micromachining of silicon.

2. Experimental materials and methods

2.1. Machine setup

SPDT experiments were performed on a 3-axis Nanoform-200 (Precitech) machine tool that is aesthetically engineered to fabricate planar, spherical, aspherical and freeform surfaces.

Table 1. Machining parameters and tool geometry used for groove making.

Cutting parameters	Values
Tool rake angle	-25^{o}
Feed rate (mm min^{-1})	2
Depth of cut (μm)	5
Spindle speed (RPM)	2000
Tool nose radius (mm)	0.2
Machining condition	Dry machining

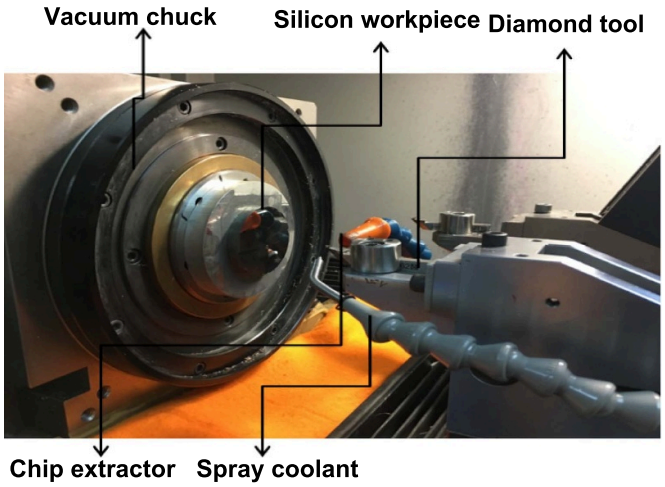

Figure 1. Experimental setup for single point diamond turning of silicon.

The SPDT experimental setup of the machine is shown in figure 1. The way it works is that a silicon wafer is held on an air bearing spindle through a vacuum chuck by an air pressure of 8–10 bar such that it self-balances and achieves thermal stability over a period of time. A diamond tool is levelled vertically and laterally using an optical tool setter and this process is referred to as the centering process. After the centering process, the tool is fed into the workpiece at a certain depth of cut at a prescribed feed rate while coolant is sprayed into the cutting zone. In this case, the coolant used was Clairsol 330. Experiments were carried out using a spindle speed of 1000 rpm, feed rate of 3 mm min^{-1} and 10 micron depth of cut.

2.2. Workpiece and tool materials

A (111) oriented single crystal silicon workpiece having Ø 45 mm and thickness 6.5 mm was used for the micromachining experiments. The diamond cutting tool with a negative rake of 10^{o} and 1.5 mm of nose radius procured from Contour Fine Tooling Ltd was used for cutting. The details of the experimental parameters used in this study are shown in tables 1–3 corresponding to groove making, plan of experiments for making groove and SPDT turning respectively.

2.3. Surface defect patterns

In the past, a variety of surface defect patterns were explored through FEA simulations during conventional turret lathe machining [9]. Two particular grooves came to light from those preliminary investigations which are being tested here. Grooves or defects made in the circumferential direction and the radial direction were generated (see figure 2) using the same SPDT experimental setup just before carrying the SPDT. These two defects, as well as the machined surface generated after the experiments, were characterised using a contact type surface profilometer (Form Talysurf PGI-120 Model from Taylor Hobson) and non-contact coherence correlation interferometer (CCI) together with a scanning electron microscope. Further details and drawings of these patterns are discussed in the next sections.

2.3.1 Circumferential direction patterns. Figure 3 shows the dimensions of grooves made in silicon with (a) 0.5 mm interspacing and (b) 1 mm interspacing. The depth of grooves was maintained as 5 microns with an opening width on the surface of about 0.1 mm. They were obtained by precise manoeuvring in the Z traverse direction. No coolant was used for better visualisation of the grooves while fabricating them. The tool movement was constrained to allow movement only in the X direction and the feed rate of 2 mm min^{-1} played a vital role in generating the fine groove profiles without any side flow as measured and characterized using the metrology tools as shown in figures 4 and 5.

2.3.2 Radial direction patterns. The patterns in the radial direction were developed in Solid Works as per the details and dimensions shown in figure 6. To fabricate these patterns, the diamond tool was mounted in such a way that the rake face approaches along the Z plane of the machine. It may be noted that the pattern generation, in this case, used the c-axis while the spindle was kept stationary. The tool was moved against the workpiece in the Z direction and scratches were made with a depth of cut of 0.3 μm and 0.5 μm at two feed rates ((a) 12 000 mm min^{-1} and (b) 1000 mm min^{-1}). The grooves generated in a straight line at two different feed rates with two different profile morphologies are shown in figure 7. By using the C axis in SPDT, the spindle was indexed by 10^{o} increment for every groove and eighteen straight line grooves were formed to mimic a star pattern. The feed rate of 12 000 mm min^{-1} yielded a better groove profile than the one obtained at the feed rate of 1000 mm min^{-1} because the dynamics of circular grooves were matched with the radial grooves at higher feed rate. For creating the circumferential patterns, the workpiece was rotated and the diamond tool was kept static yet engaged with the workpiece at a fixed depth of cut without any feed motion. Contrarily, the workpiece for creating radial patterns was kept static (headstock in brake mode) while the tool was provided an axial motion at the required depth of cut. Normally, an increasing rotation of the workpiece during turning gives a smoother finish and analogously the fast cutting operation to create radial pattern was performed by increasing the axial movement of the tool to get better finish and profile accuracies. Thus, the axial tool movement feed of 12 000 mm min^{-1} offered a better profile than 1000 mm min^{-1}. A detailed microscopic inspection of the

Table 2. Experimental plan for testing the hypothesis of surface defect machining.

Groove type	Variable parameters	Fixed machining conditions
Circumferential grooves	Circumferential spacing: 0.5 mm	Cutting tool, feed rate (2 mm min^{-1}), total depth of groove ($\sim$5 μm), dry machining. The workpiece here was rotated like turning
	Circumferential spacing: 1 mm	
Radial grooves	Feed rate: 12 000 mm min^{-1} Depth of cut: 0.3 μm	Cutting tool, angular spacing of 10^{o}, Total depth of groove ($\sim$5 μm), dry machining. The spindle here was kept stationary
	Feed rate: 1000 mm min^{-1} Depth of cut: 0.5 μm	

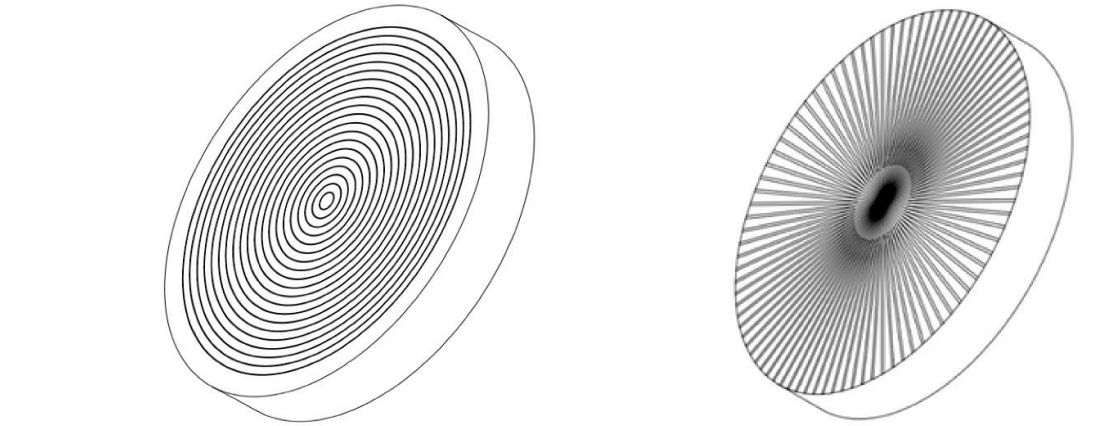

Figure 2. Schematic illustration of the two types of surface defect (grooves).

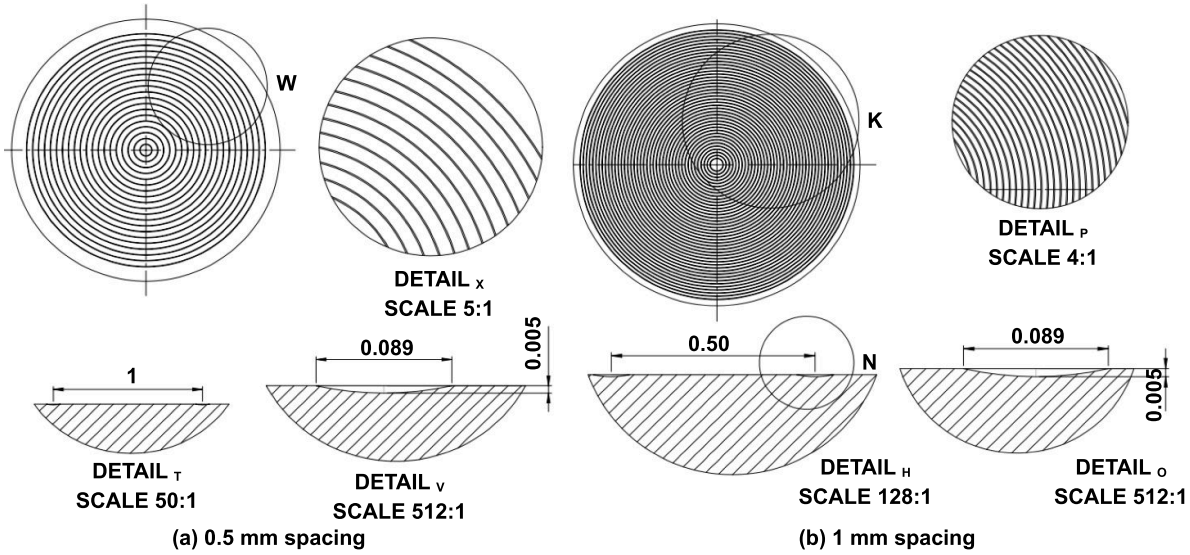

Figure 3. CAD drawing showing the details of the defects (grooves) made in circumferential direction with two different spacings: (a) 0.5 mm spacing and (b) 1 mm spacing.

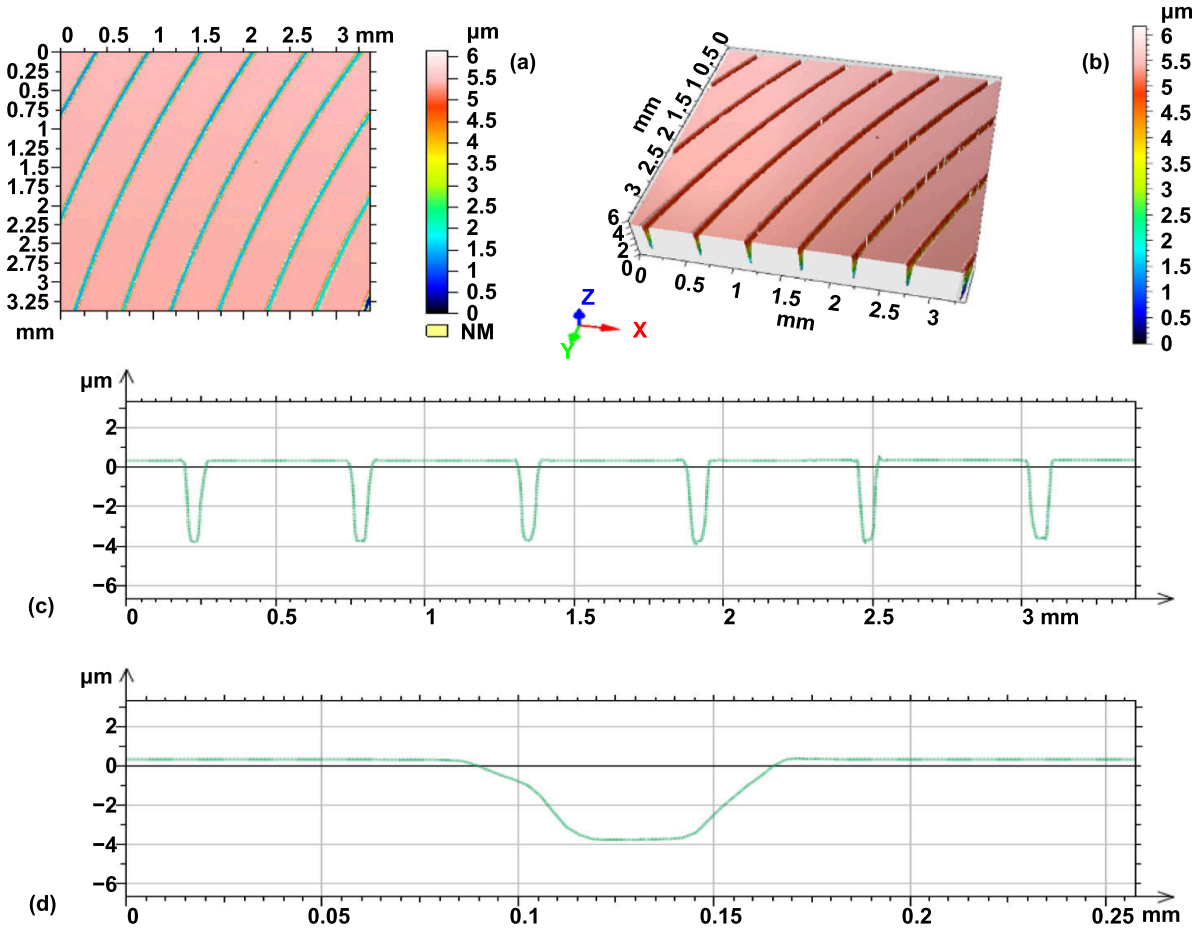

Figure 4. Cross-sectional measurements of the circumferential patterns generated by SPDT with an interspacing of 0.5 mm. (a) 2D view from the top as seen from the CCI giving an indication of the width of the groove and pattern distribution. (b) Bird's eye view to show the depth of the grooves. (c) 2D view of the section of the grooves showing the depth of grooves corresponding to the image shown in (a). (d) A detailed view of the width and depth of individual groove verifying the actual dimension of the groove.

grooves was performed using an SEM (see figure 8) to ensure that the programmable numbers were in close compliance with measured dimensions of the grooves.

3. Result obtained from the SPDT experiment and discussions

3.1. Comparison of surface roughness

3.1.1 Machining of the controlled sample using conventional SPDT method. Measurement of the surface roughness was one of the primary drivers of the work to improve the quality of machined surface obtained by SPDT. To benchmark the results of SDM incorporated SPDT, a conventional cutting trial was performed using the parameters shown in table 3. The average roughness (Ra) measured on several locations from the conventional SPDT was in the range of about 8 to 10 nm.

3.1.2 Quality of machined surface having pre-machined circumferential grooves. SDM was developed with the motivation to enhance and improve the shearing of the workpiece during cutting. A comparison of roughness parameters obtained from the machining results while providing grooves in the circumferential direction in two different cases with two interspacings of 0.5 mm and 1 mm respectively are shown in figure 9. The results for machined roughness for an interspacing of 1 mm were observed to be better than for the interspacing of 0.5 mm and there seems to be a strong correlation between this groove interspacing and the width of cut. The results hint at the fact that the interspacing should be equal to or larger than the width of the cut. It may be recalled that the width of cut is governed by the nose radius and undeformed chip thickness (cut depth in 2D) and therefore for the nose radius of 1.5 mm and depth of cut of 5 μm used in this work, 1 mm spacing seems to be better than the interspacing of 0.5 mm. An illustrative explanation of this phenomena is shown in figure 9 to show the importance of keeping the interspacing larger than the width of the cut to avoid jerky contact between the tool and the workpiece.

3.1.3 Quality of machined surface having pre-machined radial grooves. Figure 10 shows a comparison of the roughness parameters in the case of radial grooves and compares this to the previous two cases where a circumferential pattern was

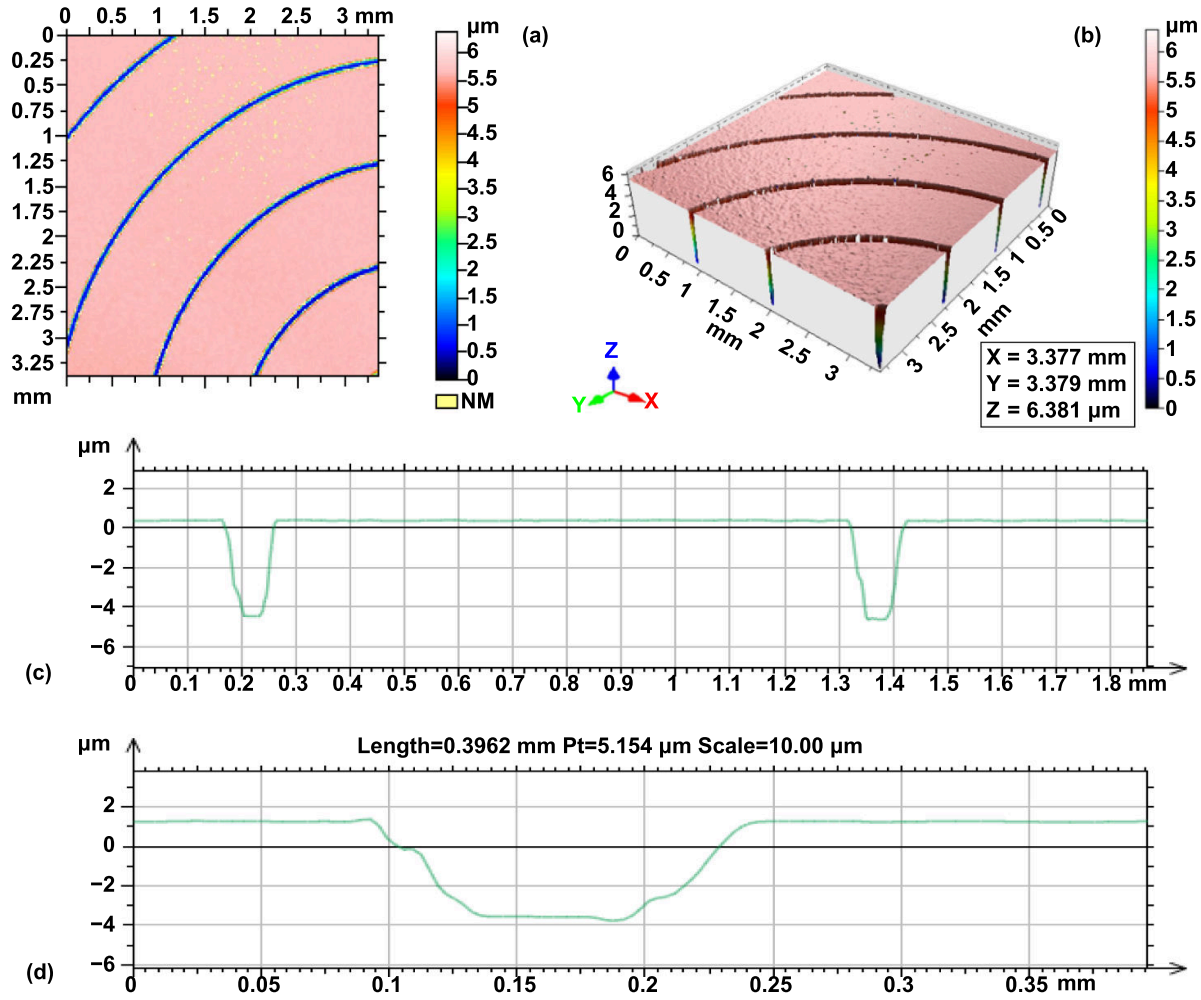

Figure 5. Cross-sectional measurements of the circumferential patterns generated by SPDT with an interspacing of 1 mm. (a) 2D view from the top as seen from the CCI giving an indication of the width of the groove and pattern distribution. (b) Bird's eye view to show the depth of the grooves. (c) 2D view of the section of the grooves showing the depth of grooves corresponding to the image shown in (a). (d) A detailed view of the width and depth of individual groove verifying the actual dimension of the groove.

Table 3. Machining parameters and tool geometry used for SPDT of silicon wafer.

Cutting parameters	Values
Tool rake angle	–10°
Feed rate (mm min^{-1})	3
Depth of cut (μm)	10
Spindle speed (RPM)	1000
Tool nose radius (mm)	1.5
Machining condition	Clairsol 330 coolant was used

provided and conventional SPDT was performed. It was found that regardless of the feed rate at which radial grooves were made, the roughness results were consistently poorer (both in terms of surface roughness and sub-surface damage) than the circumferential grooving patterns. This is the reason why in the subsequent results discussed in the paper, only a representative example of the radial groove is considered as one of the results was dropped after seeing no advantage of providing radial grooves. The average mean value of roughness (Ra) and peak to valley height (Rt) were about 8.7 nm and 664 nm during conventional SPDT and they improved when using a circumferential surface defect pattern with 1 mm spacing such that their values were about 3.2 nm and 55 nm respectively.

3.2. *Cutting chips analysis*

Investigation and analysis of cutting chip morphology forms an important aspect of machinability studies as they can reveal the underlying physical phenomena that govern the material removal process and the subsequent surface finish. The chip morphology is largely influenced by the machining conditions as well as the tool-work piece interaction pattern such as the cutting method (continuous, discontinuous or intermittent cutting), tool geometry and the material being cut. The SEM image of the chips produced during the SDM of Si in case of circumferential grooving patterns (interspacing of 0.5 mm and 1 mm) and radial grooving patterns is shown in figure 11.

As shown in figure 11(a), the nano-dust sort of chips (continuous but less width) were observed while cutting Si having

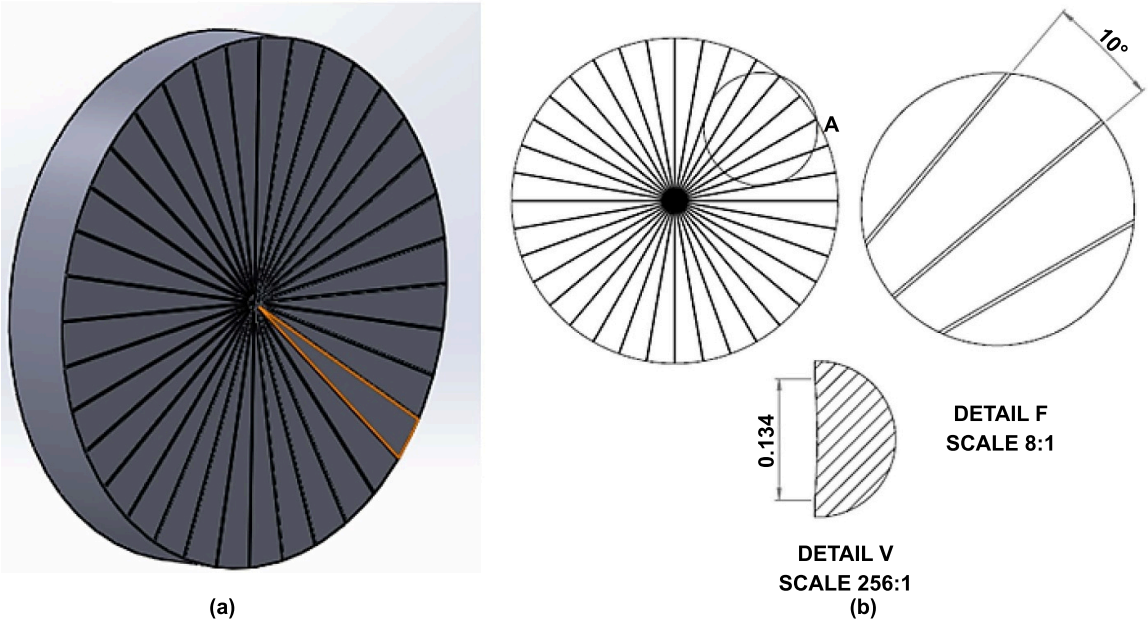

Figure 6. (a) A 3D view of the wafer showing the radial grooves made on the wafer with an angular spacing of 10^{o}. (b) Detailed dimensional 2D drawing showing the geometric measurement of each groove.

circumferential defects with 0.5 mm spacing (tool width of cut < pitch of the grooves). One can imagine that the pitch of grooves is less than the width of cut led to the partition of the chip into two pieces and the material does not attain enough plastic conditions in the process and the cutting tool and work-piece contact is somewhat jerky. Such morphological patterns in the generated chips are referred to as partially ductile chips and they can be attributed to uniform material removal rate during cutting, leading to a machined surface with moderate surface integrity. On the other hand, during SDM of Si wafer having circumferential defects with 1.0 mm spacing, the chip characteristics were found to be mid-sized and broken into few micron lengths pieces as shown in figure 11(b). This indicated healthy ductile-regime machining conditions as well as the periodic breaking of the chips (to avoid forming long continuous ribbons), which was one of the original motives behind the development of SDM that it eases cutting load by the periodic breaking of chips.

The case of SDM of Si while providing radial grooves was very different than the other two cases as the chips showed cracking, non-uniform broken size pieces as shown in figure 11(c). Such chips were striated and exemplified debris generation and conditions of cutting completely unfavourable for achieving ductile and plastic conditions.

3.3. Study of cutting chips with Raman spectroscopy

The cutting chips of the silicon wafer were examined using laser Raman spectroscopy (model—nVia Raman; make- Renishaw). The wavelength of laser used was 532 nm and the output laser power was set to 10 mW. A 20X objective lens with a numerical aperture of 0.40 was used for the measurement.

It is generally believed that loading with a hydrostatic pressure of about 10 to 12 GPa causes the crystalline silicon (Si-I) to transform to a metastable Beta tin phase of silicon (Si-II). The Beta tin phase or the Si-II phase is no more semiconductive and conducts electricity which is why this high-pressure phase transformation is said to cause metallisation of silicon and this metastable form is why metallic silicon can be machined and deformed plastically [14–16]. However, the rate of release of load (in turn cutting speed in the context of cutting) governs how this metallic form stabilises to atmospheric and room temperature phases. For example, extremely rapid unloading can cause a direct amorphisation whereas the rate of slow unloading forms other crystalline phases such as Si-XII, Si-III, Si-IV, Si-III before eventually leading to amorphisation.

In the present analysis, the pristine silicon wafer prior to machining showed a representative peak at 520 cm^{-1}. Various texts on Raman spectroscopy of silicon report the Raman peak around the value of 521 cm^{-1}. At times depending on the wafer condition or the sensitivity of the Raman instrument, a peak may show a slight shift due to the presence of residual stress (strained crystal can shift the peak to the left or right depending on the state of stress i.e. tensile or compressive).

Figure 12 shows the analysed area and the corresponding Raman spectra obtained from the selected machining zone in different cases. The peaks identified from the Raman spectra alluded to the presence of a-Si (peaks corresponding to 160 cm^{-1} and 300 cm^{-1}), crystalline Si-IV (peaks corresponding to ∼507 cm^{-1}), crystalline Si-III (peak corresponding to 170 cm^{-1}) and a-SiO2 (peaks corresponding to 263 cm^{-1}). Si-III is a BCC (bc8) form of silicon which exist between 0 to 2 GPa pressure range while Si-IV is a hexagonal diamond cubic form of silicon, which forms as a result of the martensitic transformation of Si-I (crystalline silicon)

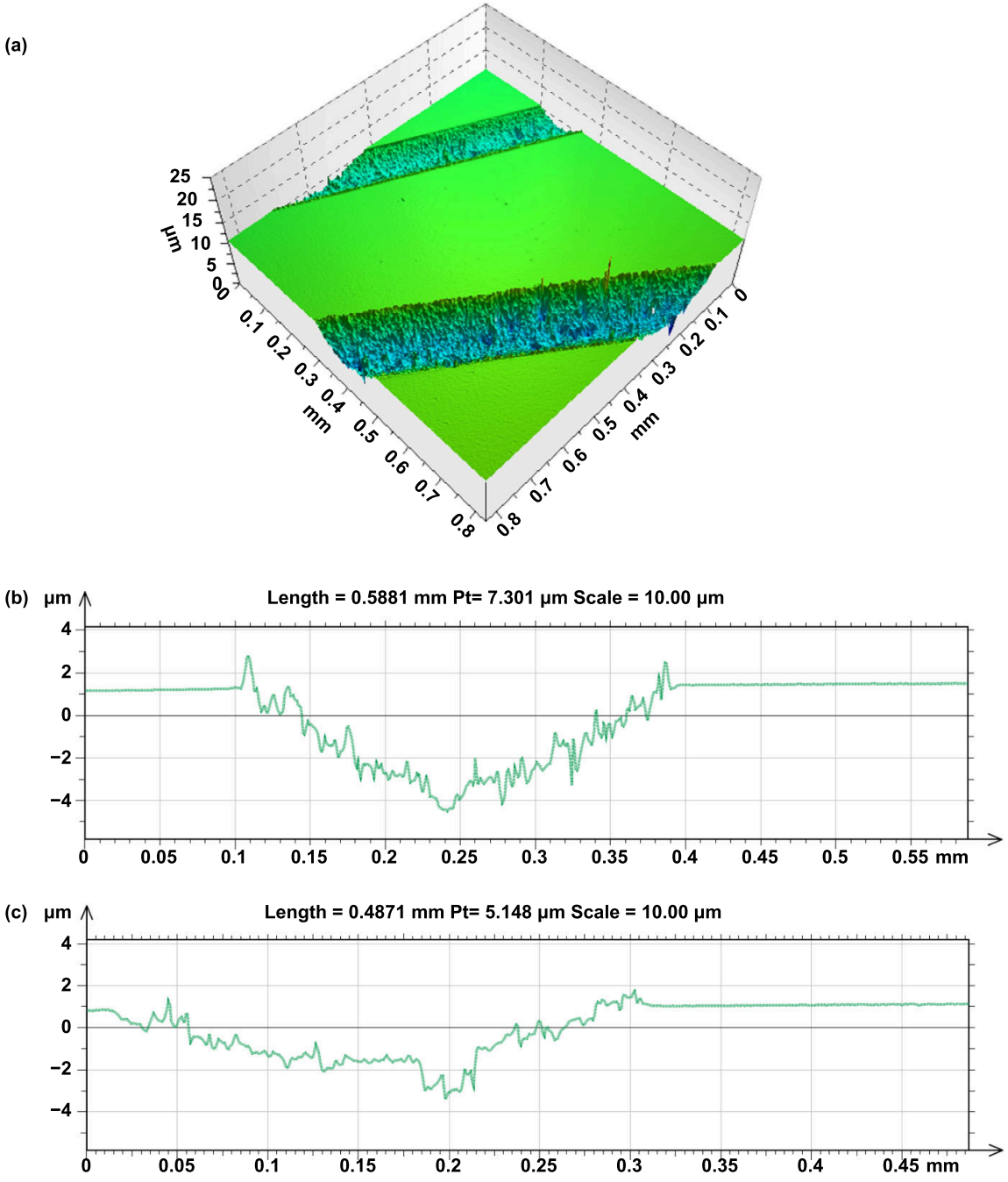

Figure 7. (a) Cross-sectional measurements of the radial patterns generated by SPDT measured by a CCI using two feed rates. (b) 2D view of the section of the groove showing the depth of groove corresponding to the feed rate of 12 000 mm min^{-1}. (c) 2D view of the section of the groove showing the depth of groove corresponding to the feed rate of 1000 mm min^{-1}, revealing an increased extent of fracture assisted material removal.

such that its relative volume becomes 0.98 with respect to Si-I [4, 17].

4. FEA of SDM of silicon

To complement the reported experimental observations, an FEA study was carried out. A three-dimensional (3D) stress dynamic explicit arbitrary Lagrangian–Eulerian (ALE) numerical model was developed using the FEA software Abaqus. In particular, the localised deformation at the contact of the tool and workpiece was modelled by using dynamic explicit ALE formulation. ALE helps to maintain the high-quality mesh during large deformation or loss of materials that generally occurs during machining. The explicit dynamic analysis procedure was based on using very small timesteps. An extensive set of prior trials were carried out to adjust the FEM solver parameters. The developed model was aimed at prediction of the machining forces, changes in shear plane

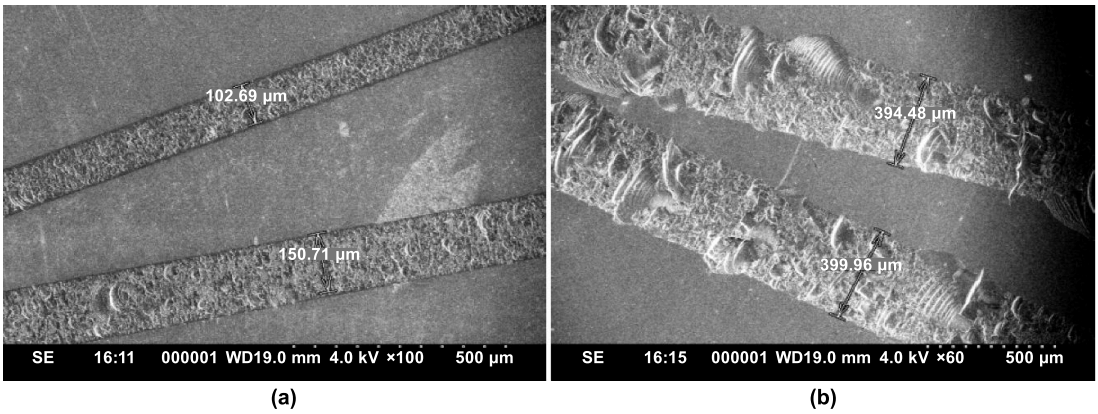

Figure 8. SEM images of radial grooves obtained at feed rate of (a) 12 000 mm min^{-1}, (b) 1000 mm/min.

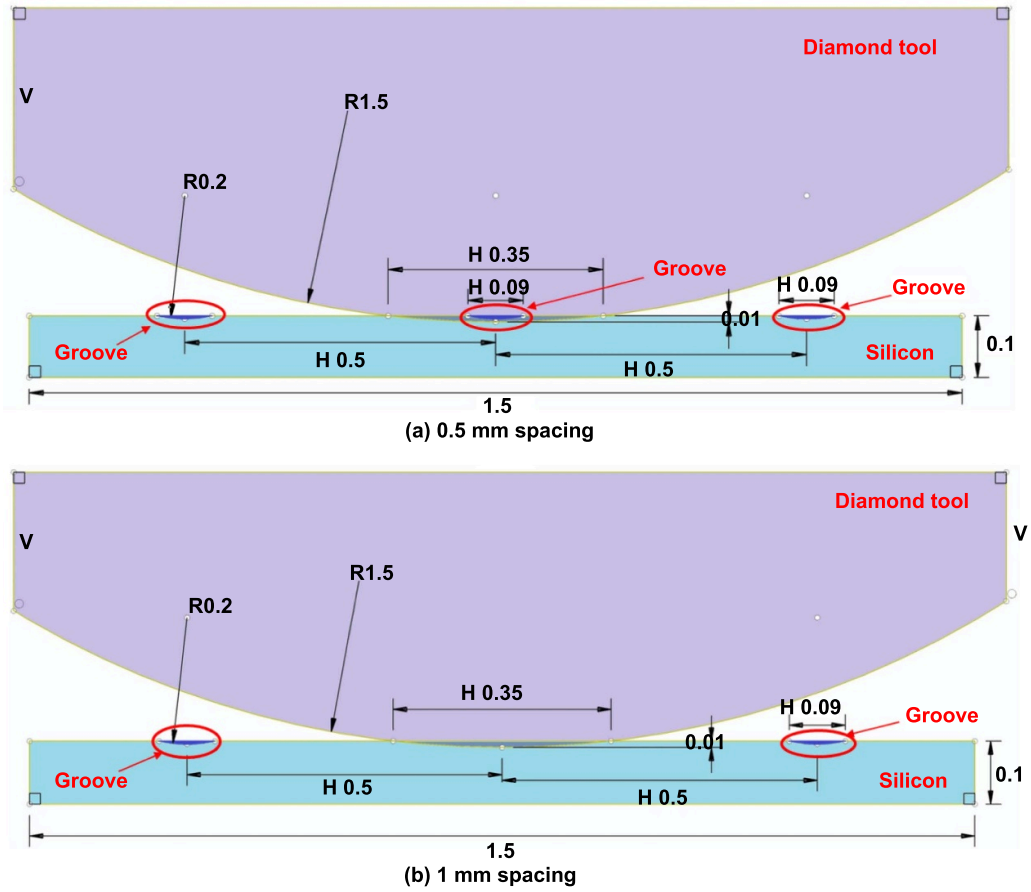

Figure 9. A schematic illustration to show the relation between interspacing of the grooves and width of cut.

angle, surface roughness and the evolution of residual stress. The model was built on the previous work by accounting for realistic material behaviour, friction consideration, damage model and by employing realistic geometry of the cutting tool [18]. Further details of the model development are discussed below.

4.1. Description and assumptions made for the simulation model development

Initially, 3D solid geometries of tool and workpiece were created. The following assumptions were made in the present model for the simplification of the process.

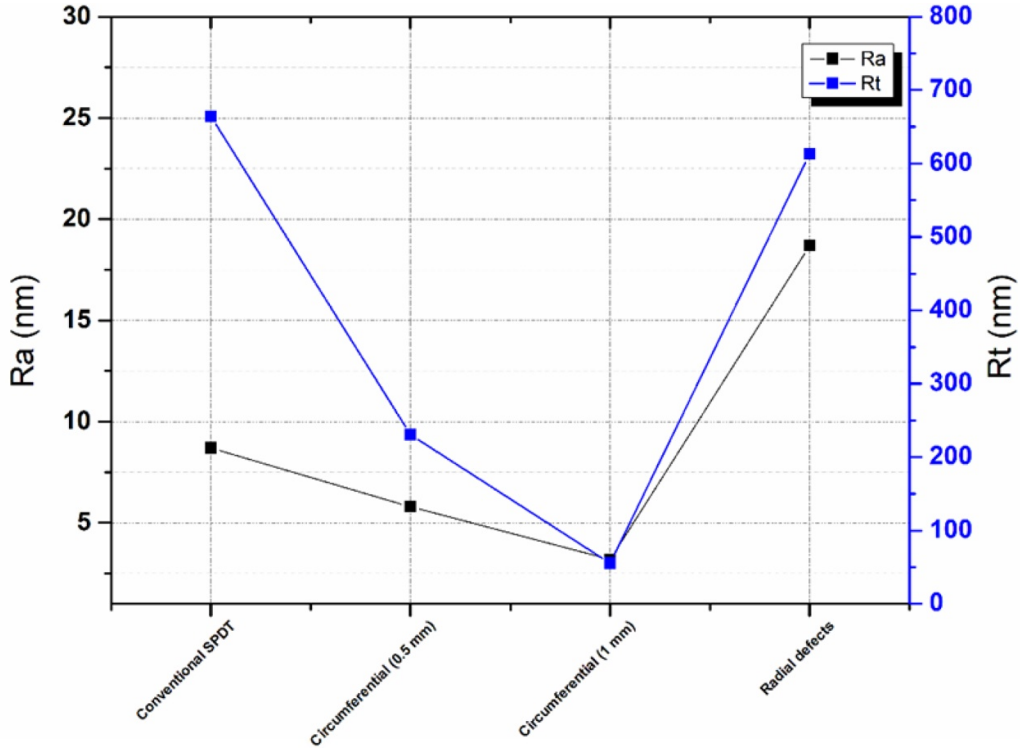

Figure 10. Comparison of the surface roughness measured using a profilometer.

- The cutting length simulated was relatively short (0.5 mm), tool wear was therefore neglected in this study.
- As the tool wear was neglected, it was modelled as a rigid body.
- For simplicity, silicon workpiece material was assumed to be isotropic and homogeneous, albeit, silicon is known to be highly anisotropic but as the simulation was an orthogonal scratch model, the effect of anisotropy was neglected.
- The workpiece material was an elastic-plastic type.
- The workpiece material was assumed to be free from initial internal residual stresses.

Figure 13 represents the schematic CAD FEM models of the SDM process developed to be simulated in a scratching mode considering the nose radius effects. The workpiece was modelled as a rectangular block with dimensions 1.5 × 0.5 × 0.1 mm. The single point diamond tool was modelled to have a -10^{o} rake angle, 10^{o} clearance angle and to 1.5 mm nose radius.

The SDM process involves non-linear, discrete and complex interactions between the tool and workpiece, as well as intense plastic deformation. Thus, it is essential to select the right type of element type in the simulation. Here, an eight-node linear bricks element (C3D8R) was chosen to mesh the tool and the workpiece. C3D8R is a general-purpose linear brick element, with reduced integration (1 integration point) and provides hourglass control and element deletion (for workpiece). The mesh density in the cutting region was kept fine whereas the region far from the cutting zone was discretized with coarser mesh. As for the boundary condition, the workpiece was constrained at the bottom to imitate the clamping action during machining. The depth of cut was set to be 10 μm and cutting velocity of 2.36 m s^{-1} was prescribed to the tool. The material properties of silicon and diamond considered in the FEA analysis are listed in table 4. As for the material constitutive model, a Johnson and Cook (J–C) model was used. The J–C constants used to simulate silicon in this work are tabulated in table 5.

FEM can simulate the chip separation naturally and therefore chip separation was achieved without introducing any physical, geometrical separation criteria or damage model. The contact between the cutting tool and the workpiece was defined by a modified Coulomb friction model. The coefficient of friction between the tool and workpiece was specified as 0.2. After the development of geometric models of workpiece and tool, material properties, the material damage law and friction law were applied. Next, the theory governing the numerical solution of FEA is presented.

4.2. Theory of the FEA numerical solver

The differential equation of motion governing the mechanical response of a system of finite elements can be written as:

$$m\ddot{u}+c\dot{u}+ku=F \tag{1}$$

where m is the mass, c is the damping coefficient, k is the stiffness coefficient.

Equation (1) in matrix form can also be written as:

$$[M]\ddot{u}+[C]\dot{u}+[K]u=[F] \tag{2}$$

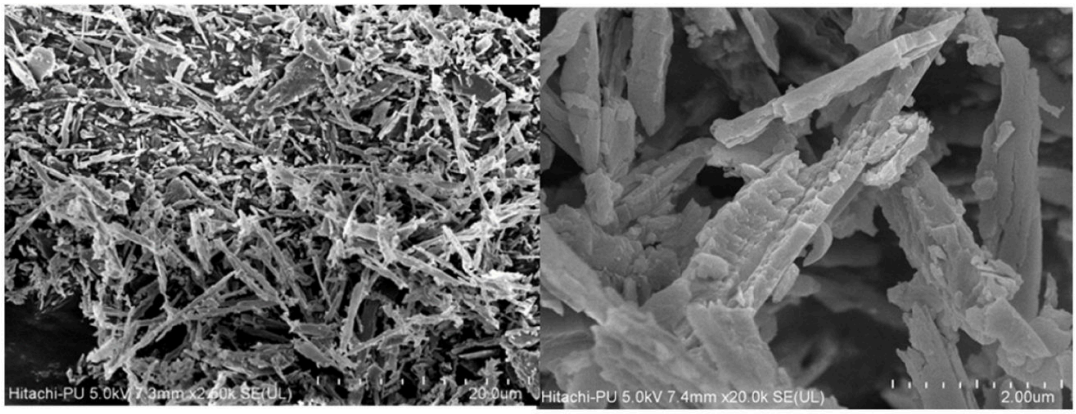

(a) Chip morphology of silicon while providing circumferential defects with 0.5 mm spacing (nano-dust kind of chips)

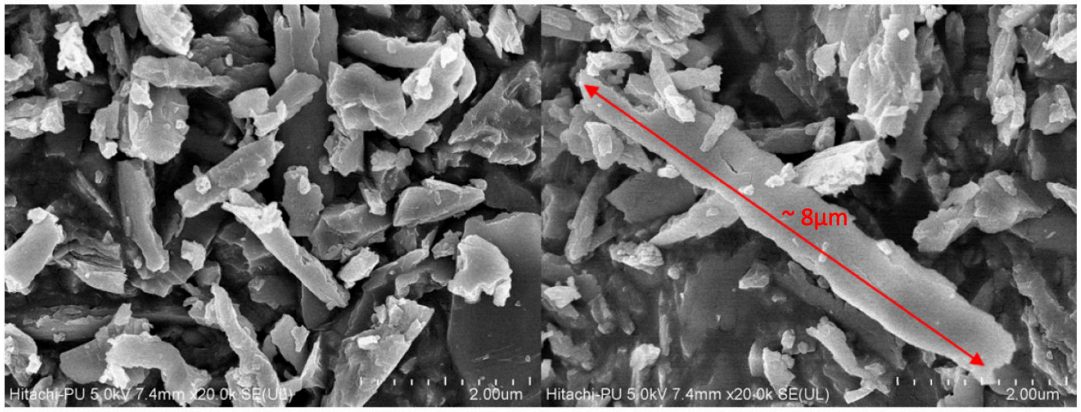

(b) Chip morphology while providing circumferential defects with 1.0 mm spacing (plastically deformed and broken)

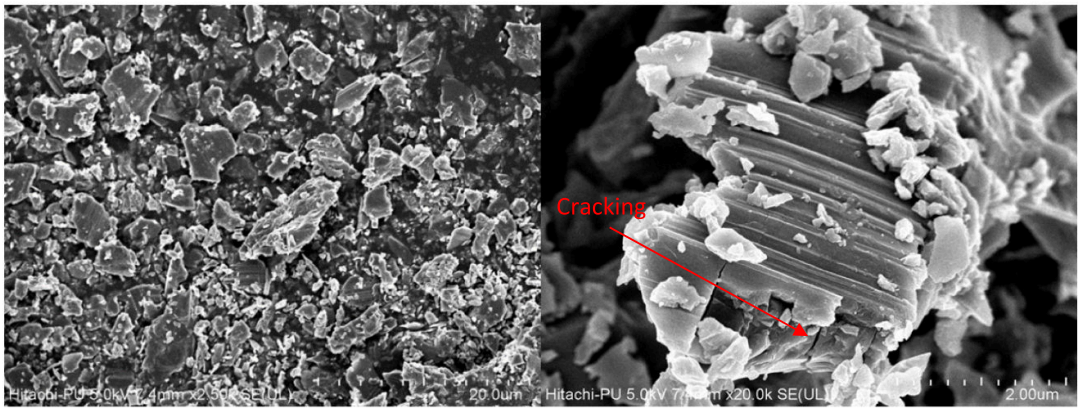

(c) Chip morphology while providing radial defects (debris kind of chipping)

Figure 11. Morphology of the silicon chips (a) and (b) circumferential grooves and (c) radial grooves.

Table 4. Material properties of diamond [19] and silicon [20].

Parameters	Unit	Diamond	Silicon
Density (ρ)	Kg m^{-3}	3350	2328
Young's modulus (E)	Gpa	1000	129.9
Poison's ratio (υ)		0.07	0.273
Thermal conductivity (k)	W $m.K^{-1}$	700	150
Thermal expansion (α)	K^{-1}	4.0×10^{-6}	2.6×10^{-6}
Specific heat (C)	J/kg.K	520	700
Melting point (T_m)	^{o}C	4373 @125kbar	1415

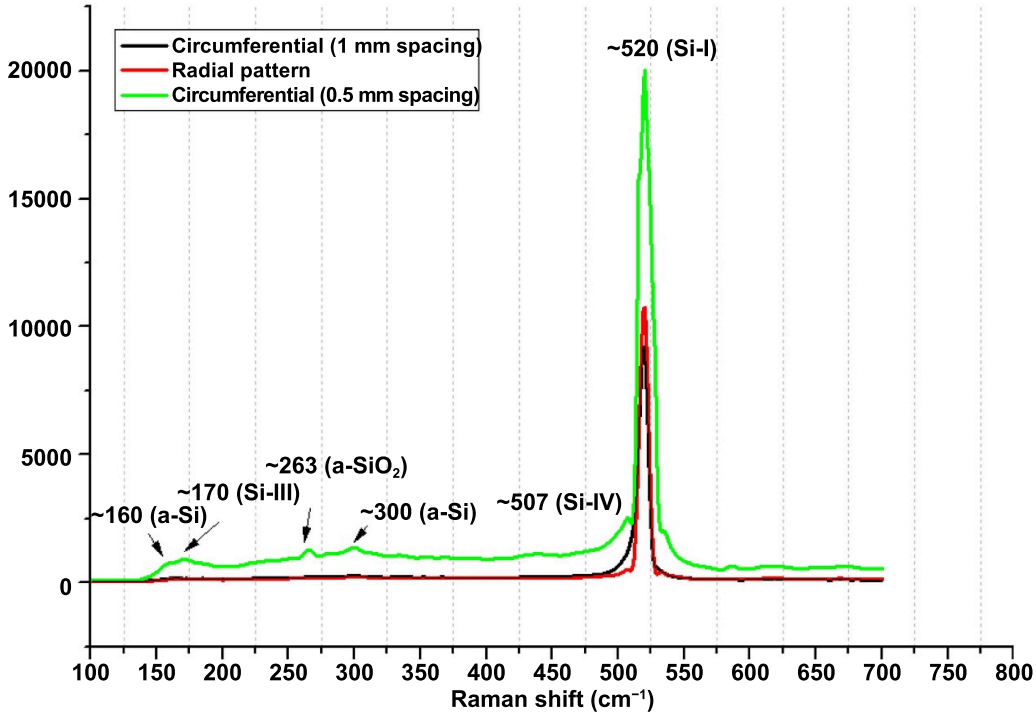

Figure 12. Raman spectra obtained after machining of three different defects exhibiting various phases of Si.

Table 5. Constants for J–C constitutive model [20].

A (MPa)	B (MPa)	C	n	m	T_m (^oC)
896.394	529.273	0.4242	0.3758	1.0	1141.85

where $[M]$ is the mass matrix, $[C]$ is the viscous damping matrix, $[K]$ is the stiffness matrix, F is the external force vector and $\ddot{u}$, $\dot{u}$ and u are the nodal acceleration, velocity and displacement vectors, respectively.

Nodal acceleration at the beginning of time increment i can be obtained by rewriting equation (2) as:

$$\ddot{u}_i = M^{-1}\left(F - C\dot{u}_i - Ku_i\right). \tag{3}$$

In the present work, explicit formulation was employed which uses central difference scheme to discretize the equations. The acceleration equation can be written as:

$$\ddot{u}_i = \frac{\dot{u}_{i+1/2} - \dot{u}_{i-1/2}}{\left(\Delta t_{i+1} + \Delta t_i\right)/2}. \tag{4}$$

Also, the velocity change is calculated by integrating the acceleration term explicitly through time using the central difference method. The change in velocity obtained is then added to velocity from the middle of the previous step and is used to calculate the velocities at the middle of the current step using:

$$\dot{u}_{i+1/2} = \left(\frac{\Delta t_{i+1} + \Delta t_i}{2}\right)\dot{u}_i + \dot{u}_{i-1/2}. \tag{5}$$

Likewise, the displacement is calculated by integrating velocity through time, which is then used to update the displacements at the end of time step using:

$$u_{i+1} = u_i + \Delta t_{i+1}\dot{u}_{1+1/12}. \tag{6}$$

Further, an explicit time integration scheme was used to solve the transient problem. It was originally developed to solve high-speed dynamic problems which were difficult to simulate using the implicit method. After the development of the numerical model, the results obtained from the numerical simulations were compared with the experimental results under similar process conditions. These are explained in the following sections.

5. Results obtained from the FEA analysis and discussions

5.1. Analysis of the machining forces, chip morphology, machining stresses and shear plane angle

At the end of the simulation (see supplementary material, available online at (https://stacks.iop.org/IJEM/02/045102/mmedia)), the cutting outputs such as forces and stresses were extracted from the simulation. Figures 14(a) and (b) show the variations in the axial cutting force or friction force (Fx) and tangential cutting force or the thrust force (Fy) during conventional cutting, cutting defects with a circumferential (circular) pattern and radial pattern. From figure 14, the cutting load can be seen to be minimal when using circumferential pattern defects.

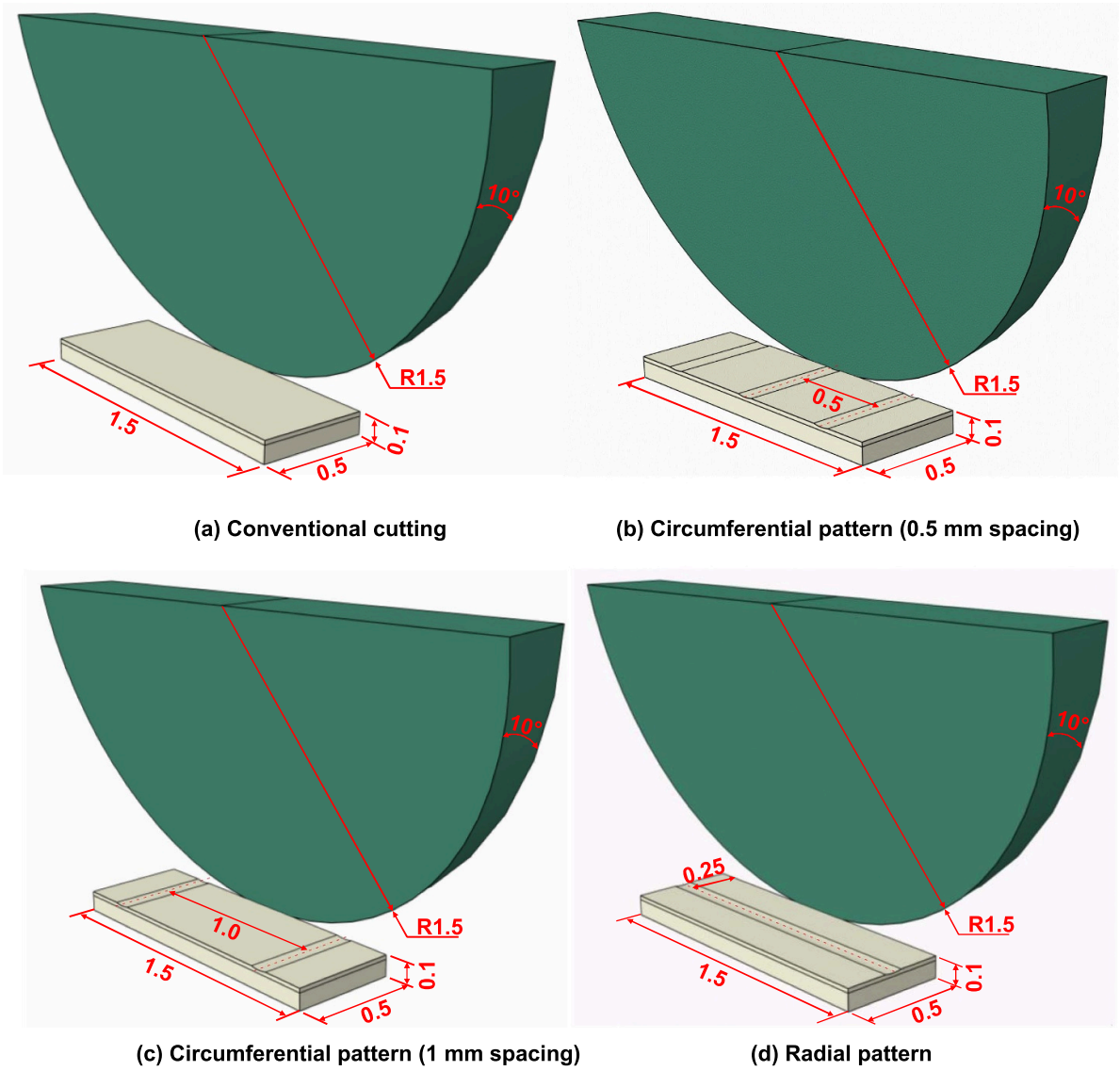

Figure 13. Work piece and tool geometries modelled to mimic the experiments showing (a) conventional cutting, (b) 1 mm spacing grooves made in circumferential pattern, (c) 0.5 mm spacing grooves made in circumferential pattern and (d) grooved made in radial pattern.

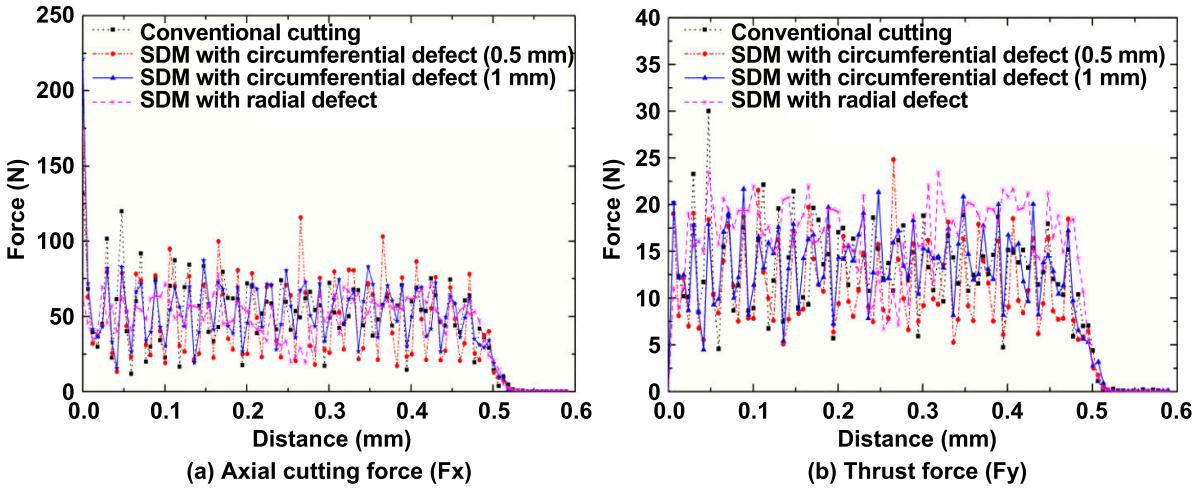

Figure 14. Simulated cutting forces obtained from conventional cutting and SDM with circumferential and radial patterns.

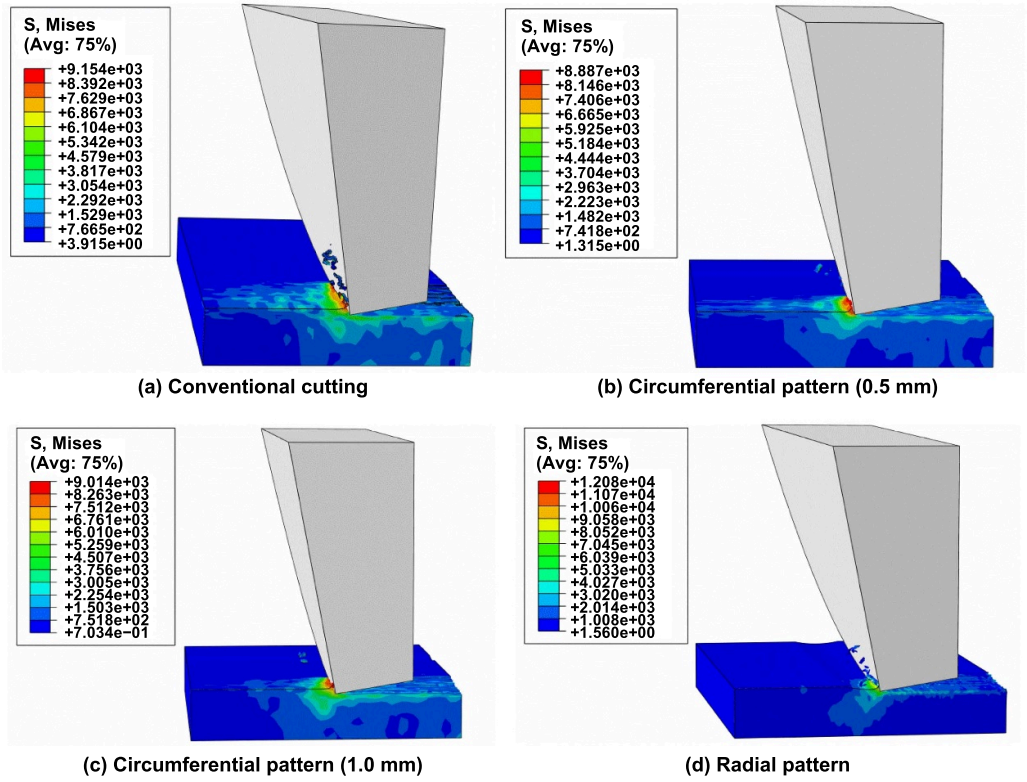

Figure 15. von Mises stress distribution in the cutting zone of silicon observed in various machining cases.

Table 6. Tangential cutting force and thrust forces for different defect types.

Machining models	Conventional cutting	Circumferential defect (0.5 mm spacing)	Circumferential defect (1 mm spacing)	Radial defect
Cutting force (N)	53.16	48.65	52.93	51.18
Thrust force (N)	13.38	11.43	13.56	16.75
Shear plane angle	52.53^{o}	48.33^{o}	50.94^{o}	56.69^{o}

Table 7. Simulated residual stress values extracted from the FEA simulations.

Machining conditions	Average residual stress (MPa)
Conventional cutting	243
SDM with circumferential patterns (0.5 mm spacing)	53
SDM with circumferential patterns (1 mm spacing)	205
SDM with radial patterns	282

Besides cutting forces, the simulation was also used to estimate the shear plane angle in each case. The shear plane angle was extracted by measuring the angle between the horizontal line and the line along the stress directions. From this analysis, the values of shear plane angle were estimated to be 52.53^{o}, 48.33^{o}, 50.94^{o} and 56.69^{o} for the cases of conventional cutting and SDM incorporated cutting with circumferential and radial patterns respectively. All these results are provided in table 6. Clearly, the shear plane, much like the cutting forces, was least while using circumferential patterns. The reduced shear plane angle shows the dominance of friction force over the normal force thus explaining the enhanced cutting action of the tool and leading to improved surface quality as observed during experiments while using circumferential defect patterns. Next in figure 15, the distribution of von Mises stress comparing conventional cutting with the SDM assisted cutting is shown. Typically, silicon was observed to yield at about 9 to 12 GPa which is consistent with the conditions of flow of silicon during micromachining reported by various papers in the past. It may be seen that the stress gradient (distribution) in the case of circumferential pattern seems more concentrated and is low compared to the other two cases. It indicates that only the cutting zone is affected by the stress and this leads to lesser sub-surface damage which would suggest differences between surface qualities of machining. The peak von Mises stress in the cutting zone was found to vary between 10 to 15 GPa in excellent correlation with the reported experimental and simulation values during ductile-mode

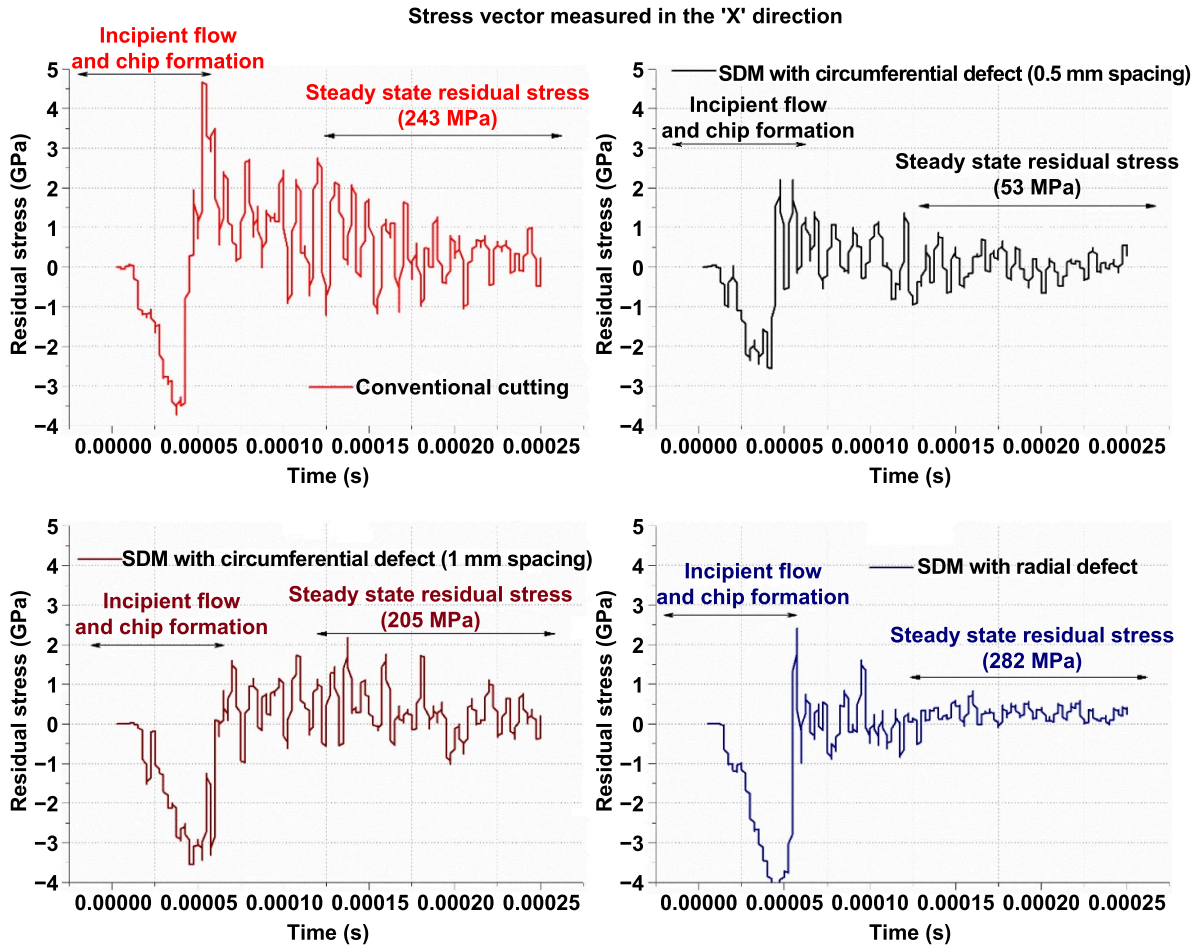

Figure 16. Evolution of the stress vector measured in the '*X*' direction of the FEA simulation showing yielding due to high compression leading to the chip formation (high negative stress), thereafter become tensile stress after the chip formation.

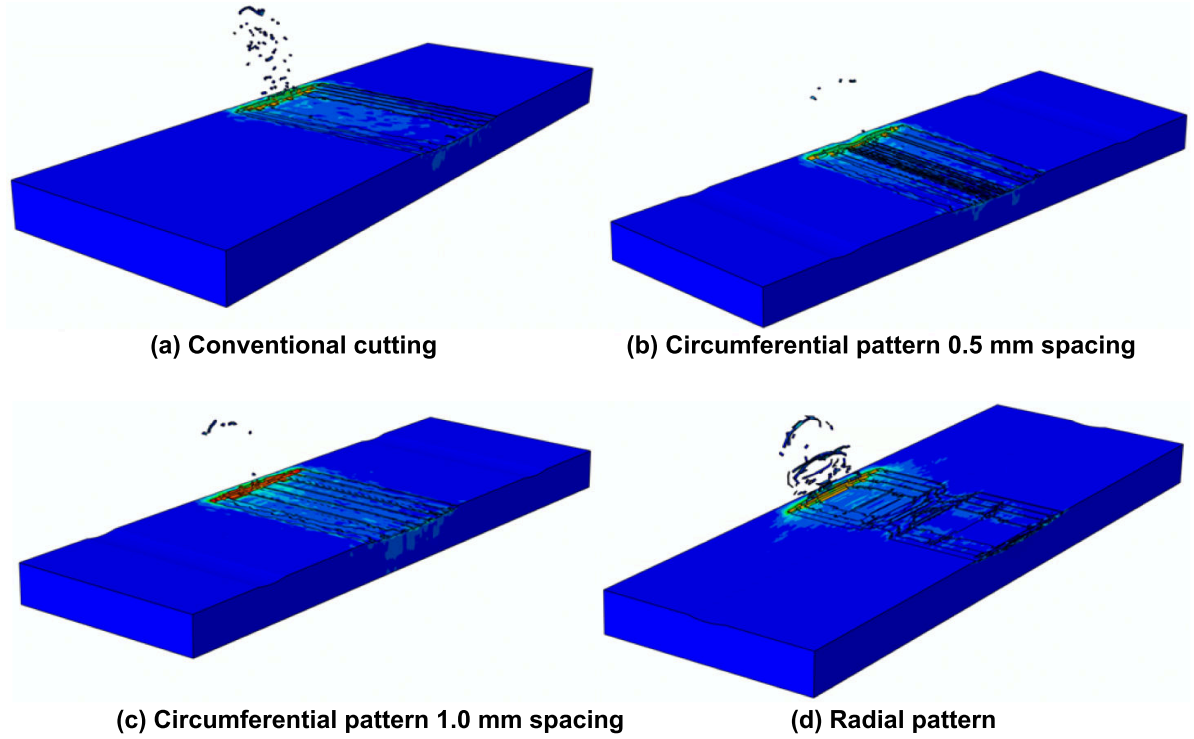

Figure 17. Simulated surface profile obtained in silicon in various machining cases (colour shows machining strain).

cutting of silicon. From the same FEA simulations, an important entity, namely, the residual stress on the machined surface was obtained by calculating the X-direction stress on the machined surface. As such, residual stress represents the extent of distortion caused on the surface due to the manufacturing process. It results due to the partial recovery of the highly strained region that undergoes high compression in the wake of the tool and recovers only partially when the tool passes by this strained zone. The development of high residual stress on the machined surface sometimes requires a post-machining process such as polishing and etching. Having a reliable simulation tool for estimation of the residual stress allows production engineers to select appropriate cutting conditions in advance to minimise these. In this study, the residual stresses were extracted from the workpiece by selecting two nodes (which were chosen to be above and below the machined surface). Table 7 corresponding to figure 16 shows the measurement of the stress vector measured in the '*X*' direction in all configurations. These stress values should not be confused with the von Mises stresses as von Mises stress is a scalar entity incorporating all stress vectors. The figure 16 data consist of two parts: (i) incipient flow stress whereby the relative region of the cutting zone experiences a high degree of compression upon being approached by the tool and (ii) the change of stress sign from negative (compression) to positive (tensile) occurs after the material separates into chips and machined surface. The stress measurement on the machine surface after chip separation was averaged, herein referred to as steady-state residual stress and being reported here in all the experiments. The residual stresses while cutting silicon with circumferential defects was lesser in magnitude in comparison to while cutting silicon in a conventional way or while providing radial defects.

Jasinevicius *et al* [21] have proposed to use $\varpi = \varpi_0 + 0.52$ L as a formula to estimate the extent of residual stress in diamond-turned silicon wafers based on their micro-Raman spectroscopy analysis of the (100) oriented silicon wafer. Here, ϖ is the experimental peak obtained using Raman spectroscopy, ϖ_0 is the theoretical characteristic peak of silicon (521.6 cm^{-1}) and L is the residual stress measured in an area in Kilobar. While cutting silicon at a depth of cut of about 0.1 μm at a feed rate of 1 μm/rev they estimated the residual stress on the machined surface to be about 221.59 MPa. The value of stress seems well compared to what is obtained from the FEA. It is noteworthy that Jasinevicius *et al* [21] observed that the residual stresses keep on decreasing with an increasing depth of cut and gradually becomes 0 while using a feed rate of 1 μm/rev and depth of cut of 10 μm. SDM with incorporating circumferential defects turns out to be useful in achieved quality of machined surface with low residual stresses.

Furthermore, it was observed that the fluctuations in the residual stresses in the case of the circumferential pattern was more periodic compared to the other configurations. This indicated the non-uniform distribution of stresses on the machined surface in the case of conventional cut and radial defects and that the stress conditions were inhomogeneous.

5.2. Qualitative analysis of the simulated surface topography

Figure 17 shows the simulated machined surface topography comparing conventional cutting with the SDM incorporated SPDT. It may be seen that the surface profile obtained from the simulation in the case of circumferential pattern seems to have more uniformity compared to conventional cutting and cutting with SDM containing radial grooves. These results can also be reasonably compared (qualitatively) to the results obtained in the experimental study. The machined surface and sub-surface during machining with SDM having radial grooves can be seen to have jerkiness or less-uniformity, which is identical to the experimental observations, where cracking in the cutting chips was observed. On the other hand, in the SDM with circumferential defects there is more homogenous cutting chip generation and the stress distribution in the cutting zone while doing SDM containing circumferential defects at a spacing of 1 mm seems most focused compared to all other cutting configurations. Overall, it seems that the circumferential patterned defects produced better surface finish with less damage and defects in the sub-surface.

6. Conclusions

An experimental and numerical simulation investigation was pursued to highlight the underlying benefits of using SDM of silicon, which is classed as a nominally hard, brittle material. In the past, the SDM method was found to work successfully while machining hard steels by virtue of a reduced shear plane angle but the current investigation now shows that even ductile-mode machining of silicon can be improved by embracing the concept of SDM into diamond turning. Taking an example of the (111) surface of a silicon wafer, two types of surface defects were made (circumferential and radial directional grooves) and the quality of machining in both cases was benchmarked to conventional SPDT.

(a) The incorporation of SDM into the diamond turning of silicon provided favourable advantages over conventional diamond turning of silicon. The direction and orientation of surface defects to leverage this additional advantage are critical, for instance, prior machining defects made in the circumferential direction of the wafer, was observed to contribute to improving the cutting performance compared to SDM with radial patterns. The radial patterns deteriorated the quality of machining while machining silicon.

(b) Cutting chip morphology showed distinct patterns for example, the SDM with radially patterned grooves resulted in striated featured chips and debris arising from brittle fracture. In comparison to this, the circumferential pattern showed improved ductility, however, the importance of width of cut was shown to be larger than the interspacing of the grooves was recognised to be an essential condition to get fully desirable benefits of the SDM incorporate SPDT of brittle materials.

(c) Laser Raman spectroscopy revealed amorphisation of silicon as well as the presence of Si-IV and a-SiO_2 phases confirming the influential role of tribo-chemistry during precision machining of silicon with a diamond tool.

Overall, this novel work on surface defect incorporated machining of silicon has opened new possibilities to apply this technique to a wider range of other hard, brittle materials such as SiC, ZnSe and GaAs as well as hard steels. Care must be taken to optimise the geometry of surface defects together with the machining parameters to obtain full advantages of SDM.

Data statement

All data in the manuscript will be available through Cranfield University data repository (10.17862/cranfield.rd.12442886).

Acknowledgments

N K acknowledges financial support provided by CSIR, India through the project grant MLP0056 and Director, CSIR-CSIO for his support and encouragement. N K is also grateful to Dr Vinod Karar in providing infrastructural support in carrying out the experiments.

SG acknowledges the financial support provided by the UKRI via Grants Nos. EP/L016567/1, EP/S013652/1, EP/S036180/1, EP/T001100/1 and EP/T024607/1, Royal Academy of Engineering via Grants Nos. IAPP18-19\295, TSP1332 and EXPP2021\1\277, EURAMET EMPIR A185 (2018), H2020 EU Cost Actions (CA15102, CA18125, CA18224 and CA16235) and Newton Fellowship award from the Royal Society (NIF\R1\191571).

The work used Isambard Bristol, UK supercomputing service accessed by Resource Allocation Panel (RAP) grant as well as ARCHER resources.

ORCID iDs

Xichun Luo https://orcid.org/0000-0002-5024-7058
Saurav Goel https://orcid.org/0000-0002-8694-332X

References

[1] Blackley W S and Scattergood R O 1994 Chip topography for ductile-regime machining of germanium *J. Manuf. Sci. Eng.* **116** 263–6
[2] Shibata T, Fujii S, Makino E and Ikeda M 1996 Ductile-regime turning mechanism of single-crystal silicon *Prec. Eng.* **18** 129–37
[3] Randall T, Walter J J H, Scattergood R and Nemanich R 2009 High pressure phase transformation and ductility in diamond turned single crystal silicon *North Carolina State University Raleigh* NC27695Y7918
[4] Goel S, Kovalchenko A, Stukowski A and Cross G 2016 Influence of microstructure on the cutting behaviour of silicon *Acta Mater.* **105** 464–78
[5] Goel S, Luo X C, Reuben R L and Pen H M 2012 Influence of temperature and crystal orientation on tool wear during single point diamond turning of silicon *Wear* **284-5** 65–72
[6] Yan J W, Syoji K, Kuriyagawa T and Suzuki H 2002 Ductile regime turning at large tool feed *J. Mater. Process. Technol.* **121** 363–72
[7] Chavoshi S Z, Goel S and Morantz P 2017 Current trends and future of sequential micro-machining processes on a single machine tool *Mater. Des.* **127** 37–53
[8] Rashid W B and Goel S 2016 Advances in the surface defect machining (SDM) of hard steels *J. Manuf. Process.* **23** 37–46
[9] Rashid W B, Goel S, Luo X C and Ritchie J M 2013 The development of a surface defect machining method for hard turning processes *Wear* **302** 1124–35
[10] Rashid W B, Goel S, Luo X C and Ritchie J M 2013 An experimental investigation for the improvement of attainable surface roughness during hard turning process *Proc. Inst. Mech. Eng.* B **227** 338–42
[11] Goel S, Rashid W B, Luo X C, Agrawal A and Jain V K 2014 A theoretical assessment of surface defect machining and hot machining of nanocrystalline silicon carbide *J. Manuf. Sci. Eng.* **136** 021015
[12] Komanduri R, Lee M, Flom D G, Thompson R A, Jones M G and Douglas R J 1982 Pulse laser pretreated machining. *US Patent* 4356376
[13] Mir A, Luo X C and Siddiq A 2017 Smooth particle hydrodynamics study of surface defect machining for diamond turning of silicon *Int. J. Adv. Manuf. Technol.* **88** 2461–76
[14] Mylvaganam K, Zhang L C, Eyben P, Mody J and Vandervorst W 2019 Evolution of metastable phases in silicon during nanoindentation: mechanism analysis and experimental verification *Nanotechnology* **20** 305705
[15] Smith G S, Tadmor E B and Kaxiras E 2000 Multiscale simulation of loading and electrical resistance in silicon nanoindentation *Phys. Rev. Lett.* **84** 1260–3
[16] Smith G S, Tadmor E B, Bernstein N and Kaxiras E 2001 Multiscale simulations of silicon nanoindentation *Acta Mater.* **49** 4089–101
[17] Goel S, Luo X C, Agrawal A and Reuben R L 2015 Diamond machining of silicon: a review of advances in molecular dynamics simulation *Int. J. Mach. Tools Manuf.* **88** 131–64
[18] Goel S, Llavori I, Zabala A, Giusca C, Veldhuis S C and Endrino J L 2018 The possibility of performing FEA analysis of a contact loading process fed by the MD simulation data *Int. J. Mach. Tools Manuf.* **134** 79–80
[19] Mariayyah R 2007 Experimental and numerical studies of ductile regime machining of silicon carbide and silicon nitride *PhD Thesis* (Charlotte, NC: The University of North Carolina at Charlotte)
[20] Venkatachalam S 2007 Predictive modeling for ductile machining of brittle materials *PhD Thesis* (Atlanta, GA: Georgia Institute of Technology)
[21] Jasinevicius R G, Duduch J G, Montanari L and Pizani P S 2008 Phase transformation and residual stress probed by Raman spectroscopy in diamond-turned single crystal silicon *Proc. Inst. Mech. Eng.* B **222** 1065–73

2020-07-31

Surface defects incorporated diamond machining of silicon

Khatri, Neha

IOP

Khatri N, Barkachary BM, Muneeswaran B, et al., (2020) Surface defects incorporated diamond machining of silicon. International Journal of Extreme Manufacturing, Volume 2, Issue 4, December 2020, Article number 045102

https://doi.org/10.1088/2631-7990/abab4a